PAPER

# Moiré superlattice-level stick-slip instability originated from geometrically corrugated graphene on a strongly interacting substrate

To cite this article: Ruoyu Shi *et al* 2017 *2D Mater.* **4** 025079

View the article online for updates and enhancements.

Related content

- Thickness dependent friction on few-layer MoS2, WS2, and WSe2
  Liang Fang, Da-Meng Liu, Yuzheng Guo et al.
- Superlubricity of two-dimensional fluorographene/MoS2 heterostructure: a first-principles study
  Lin-Feng Wang, Tian-Bao Ma, Yuan-Zhong Hu et al.
- Molecular assembly on two-dimensional materials
  Avijit Kumar, Kaustuv Banerjee and Peter Liljeroth

Recent citations

- Lateral force modulation by moiré superlattice structure: Surfing on periodically undulated graphene sheets
  Jun Liu *et al*

This content was downloaded from IP address 159.226.35.207 on 03/11/2017 at 17:01

2D Materials

PAPER

RECEIVED
6 February 2017

REVISED
6 April 2017

ACCEPTED FOR PUBLICATION
18 April 2017

PUBLISHED
28 April 2017

# Moiré superlattice-level stick-slip instability originated from geometrically corrugated graphene on a strongly interacting substrate

Ruoyu Shi[1,7], Lei Gao[1,2,7], Hongliang Lu[3,4], Qunyang Li[1,5], Tian-Bao Ma[1], Hui Guo[3,4], Shixuan Du[3,4], Xi-Qiao Feng[1,5], Shuai Zhang[5], Yanmin Liu[1], Peng Cheng[6], Yuan-Zhong Hu[1], Hong-Jun Gao[3,4] and Jianbin Luo[1]

[1] State Key Laboratory of Tribology, Tsinghua University, Beijing 100084, People's Republic of China
[2] Corrosion and Protection Center, Key Laboratory for Environmental Fracture (MOE), University of Science and Technology Beijing, Beijing 100083, People's Republic of China
[3] School of Physical Sciences, University of Chinese Academy of Sciences, Beijing 100049, People's Republic of China
[4] Institute of Physics, Chinese Academy of Sciences, Beijing 100190, People's Republic of China
[5] AML, CNMM, School of Aerospace Engineering, Tsinghua University, Beijing 100084, People's Republic of China
[6] Asylum Research, Santa Barbara, CA 93117, United States of America
[7] These authors contributed equally to this work.

The authors declare no competing financial interest.

**E-mail:** qunyang@tsinghua.edu.cn, mtb@mail.tsinghua.edu.cn and luojb@tsinghua.edu.cn

**Keywords:** stick-slip, moiré structure, interfacial interaction, friction control

Supplementary material for this article is available online

## Abstract

Two dimensional (2D) materials often exhibit novel properties due to various coupling effects with their supporting substrates. Here, using friction force microscopy (FFM), we report an unusual moiré superlattice-level stick-slip instability on monolayer graphene epitaxially grown on Ru(0 0 0 1) substrate. Instead of smooth friction modulation, a significant long-range stick-slip sawtooth modulation emerges with a period coinciding with the moiré superlattice structure, which is robust against high external loads and leads to an additional channel of energy dissipation. In contrast, the long-range stick-slip instability reduces to smooth friction modulation on graphene/Ir(1 1 1) substrate. The moiré superlattice-level slip instability could be attributed to the large sliding energy barrier, which arises from the morphological corrugation of graphene on Ru(0 0 0 1) surface as indicated by density functional theory (DFT) calculations. The locally steep humps acting as obstacles opposing the tip sliding, originates from the strong interfacial electronic interaction between graphene and Ru(0 0 0 1). This study opens an avenue for modulating friction by tuning the interfacial atomic interaction between 2D materials and their substrates.

## 1. Introduction

Friction is the conversion of mechanical energy of sliding bodies into heat and other excitations [1], and is one of the most fundamental and ubiquitous processes in nature. To control friction efficiently and reliably is desirable at all length scales, especially at the small scales, where the surface forces such as friction and adhesion dominate the performance and sustainability of the electromechanical systems (MEMS/NEMS) [2]. Two-dimensional (2D) materials with atomically-thin architectures and novel properties, provide promising prospects for friction control and lubrication in small scale devices [3–10]. In the past decade, a series of characteristics, such as the out-of-plane bending stiffness, the interlayer registry, the electron-phonon coupling, the chemical modifications, have been reported to either enhance or diminish friction energy dissipation of 2D materials at the nanoscale [3, 11–16].

The properties of 2D materials can also be tailored by positioning on various substrates, or layer-by-layer stacking constituting 2D heterostructures [17–21]. Specifically, moiré superlattices are formed when 2D materials are covered on crystalline substrates with matching hexagonal symmetry and intrinsic lattice mismatch or orientational misalignment, showing extraordinary modulation of topography [18, 22], electronic

© 2017 IOP Publishing Ltd

[18, 23], optical properties [24], as well as mechanical properties [25–29] of the 2D materials. Previous study has shown long-range modulations of friction via moiré superlattices in graphene based heterostructures [30–33], which could be described by the Prandtl–Tomlinson (PT) model with a superimposed long-range 'super-potential' [34]. However, to the best of our knowledge, the existing experimental and theoretical studies only report smooth and subtle long-range friction modulation. Fundamental questions still remain open to achieve widely tunable frictional characteristics of 2D materials and to reveal the physical origins of the modulation effects: Whether the moiré superstructure could invoke long-range stick-slip instabilities on 2D materials? Whether these 'super-potential' corrugations originate from geometric or electronic corrugation of 2D heterostructures?

By intentionally selecting graphene/Ru(0 0 0 1) architecture with strong interfacial coupling, we reported for the first time that stick-slip instability could occur at dual-scales simultaneously by high-resolution friction force microscopy, i.e. a shorter scale with the regular atomic periodicity, and a larger scale with the moiré superlattice periodicity invoking an additional friction dissipation channel. The origin of this superlattice-level instability, as suggested by the potential energy surface (PES) estimation by density functional theory (DFT) calculations, is attributed to an extraordinarily large sliding energy barrier due to the periodically corrugated topography of graphene, which is primarily determined by the strong interfacial electronic interaction between graphene and Ru(0 0 0 1). The persistence of this corrugated structure against high external normal loads verifies the robustness of the superlattice-level stick-slip instability. The interfacial coupling with substrate plays an important role in controlling the frictional properties of 2D materials. Switching from significant superlattice-level stick-slip instability to continuous modulation is achieved by replacing the strongly interacting Ru(0 0 0 1) substrate by weakly interacting Ir(1 1 1) substrate. Our study provides a new method to control nanoscale friction by tuning the interfacial atomic interaction between atomically thin layers and various supporting substrates.

## 2. Methods

### 2.1. Fabrication of graphene/Ru(0 0 0 1) sample

The graphene/Ru(0 0 0 1) sample was fabricated by thermal decomposition of ethylene on single crystal Ru(0 0 0 1) substrate. Before growth of graphene, Ru(0 0 0 1) sample was cleaned by several cycles of Ar ion sputtering followed by annealing at 900 °C. The Ru(0 0 0 1) surface was confirmed clean by low energy electron diffraction (LEED) with sharp diffraction spots. Then Ru substrate was heated to 850 °C and exposed to ethylene (partial pressure $1.4 \times 10^{-4}$ Pa) for 100 s. After cooling down, the quality of graphene was checked again by LEED, which showed clear diffraction spots from graphene/Ru(0 0 0 1) moiré pattern.

### 2.2. Friction measurement

The lateral force images of graphene on Ru(0 0 0 1) were obtained by AFM contact mode (Cypher AFM, Oxford Instruments, under atmospheric environment, temperature ~25 °C). A silicon AFM probe (Olympus AC240, specified tip radius $R = 8$ nm, force constant $k = 2.10 \pm 0.15$ N m$^{-1}$, lateral sensitivity $\alpha = 5.23 \pm 0.35$ nN mV$^{-1}$) was used to obtain a 20 nm lateral force map, and the normal load of 740 nN was imposed on the graphene and the scanning velocity was set to 0.78 $\mu$m s$^{-1}$. 2 nm lateral force maps were obtained by a silicon AFM probe (Bruker SNL, specified tip radius $R = 8$ nm, normal force constant $k = 0.19 \pm 0.03$ N m$^{-1}$, lateral sensitivity $\alpha = 2.20 \pm 0.40$ nN mV$^{-1}$) at a normal load of 84 nN and a velocity of 0.06 $\mu$m s$^{-1}$. Normal force constant was calibrated with thermal noise method [35]. Lateral sensitivity was calibrated by a diamagnetic lateral force calibrator [36]. The lateral stiffness of the probe is measured and estimated to be $37.04 \pm 3.10$ N m$^{-1}$ for AC240 and $26.00 \pm 4.60$ N m$^{-1}$ for SNL, according to the method described in literature [37].

### 2.3. Calculation methods

The density functional theory (DFT) calculations were implemented in the Vienna *ab initio* Simulation Package (VASP) [38]. The projector-augmented-wave (PAW) method was utilized to model the core electrons [39]. A non-local optB86b-vdW exchange-correlation functional was used and the selection of this functional was due to its ability to approximately describe the dispersion interaction (van der Waals forces) and it has been demonstrated to be currently among the most accurate vdW functional [40–42]. The plane wave basis kinetic energy cut off was set to 400 eV.

The 3.0 nm supercell ($12 \times 12$ unit cells of graphene sitting on $11 \times 11$ unit cells of Ru) was selected for the calculation since it is more stable than the 2.7 nm supercell ($11 \times 11$ unit cells of graphene sitting on $10 \times 10$ unit cells of Ru) [43]. The supercell contains three layers Ru (0 0 0 1) lattices and monolayer graphene with a vacuum layer of 22 Å. The graphene and first Ru (0 0 0 1) layer were allowed to relax until the forces on all the relaxed atoms were less than 0.02 eV Å$^{-1}$. All the calculations were done using experimental Ru lattice constants ($a = 2.7058$ Å and $c = 4.2816$ Å).

## 3. Results and discussion

Figure 1(a) shows a high-resolution lateral force image of graphene on Ru(0 0 0 1) under a normal force of 740 nN, where a long-wavelength modulation can be clearly observed in addition to the regular atomic stick-slip friction. This modulation was found to be a manifestation of a long-range stick-slip as indicated by the friction loop shown in figures 1(b) and (c). For the blue scan line in figure 1(a), three stages can be roughly distinguished as indicated by the lateral force profiles: (1) a long-range stick stage with overall lateral force ascending near-linearly, (2) a slip stage

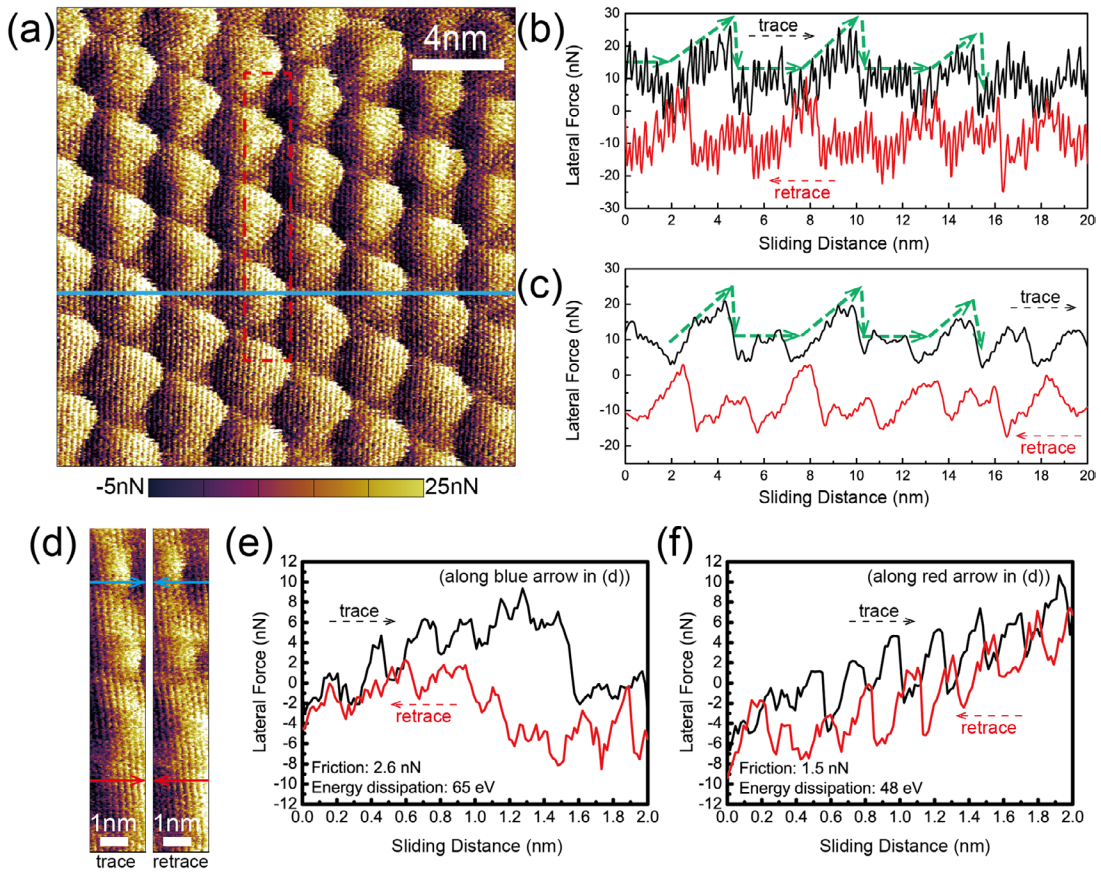


**Figure 1.** (a) Lateral force map on graphene/Ru(0 0 0 1) heterostructure. A silicon AFM probe (Olympus AC240, specified tip radius $R = 8$ nm, normal force constant $k = 2.10 \pm 0.15$ N m$^{-1}$, lateral sensitivity $\alpha = 5.23 \pm 0.35$ nN mV$^{-1}$) was used at a normal load of 740 nN. (b) Friction loop along the blue line in (a). (c) Friction loop after smoothing on (b) with the Savitzky–Golay method. The horizontal axes represent the displacement of the cantilever base relative to the sample surface. Additional experimental evidence with varied scan sizes confirms the coexistence of this dual-wavelength stick-slip behaviors rather than artifacts (see supporting information). (d) Lateral force map in a small range of 2 nm in fast scan direction (in a region similar to the red dotted frame in (a)). A silicon AFM probe (Bruker SNL, specified tip radius $R = 8$ nm, typical normal force constant $k = 0.19 \pm 0.03$ N m$^{-1}$, lateral sensitivity $\alpha = 2.20 \pm 0.40$ nN mV$^{-1}$) was used at a normal load of 84 nN. (e) Friction loop along the blue arrow in (d) with the tip sliding across the moiré pattern. (f) Friction loop along the red arrow in (d) with the tip sliding inside the moiré pattern. Average friction and energy dissipation are denoted in the case of (e) and (f).

with sudden drop in lateral force, and (3) a stable sliding stage with only atomic stick-slip motion. The long-range stick-slip behavior results in a periodic pattern with a six fold symmetry in the lateral force image, with a period about 3 nm. Besides, both the atomic and superstructure periodicity and the misfit angle between them could be deduced according to the results of Fourier transform (see supporting information (stacks.iop.org/TDM/4/025079/mmedia)). This period coincides with the periodicity of moiré superlattice for graphene/Ru(0 0 0 1) as previously measured by scanning tunneling microscopy (STM) [44].

As unstable motion is often associated with energy dissipation [45], the superlattice-level slip instability also introduces a new dissipation mode in our graphene/Ru system. To illustrate this idea, we reduced the scan size to 2 nm (less than the superlattice periodicity) and slid at different locations, as indicated in figure 1(d), such that friction traces either with or without a superlattice-level slip could be obtained as shown in figures 1(e) and (f). When a scan does not include a superlattice-level slip, the trace and retrace curves are close to each other showing only atomic-level stick-slip. The energy dissipation in this case is primarily attributed to the atomic-level stick-slip. However, when a scan includes a superlattice-level slip the long-range slip process leads to an obvious hysteresis and 35% more energy dissipation as estimated from the enclosed area of the friction loop.

The dual-scale stick-slip behavior can be captured by the 2D Prandtl–Tomlinson (PT) model [46] with a dual-wavelength potential energy landscape as shown in figure 2(a). The tip-sample interaction potential $U_{\text{hetero}}(x, y)$ could be described as superposition of two independent potential energy surfaces: (1) the graphene lattice-level potential by $U_{\text{lat}}(x, y)$ in equation (1), periodically duplicated according to the atomic positions; and (2) the superlattice-level potential by $U_{\text{sup}}(x, y)$ in equation (2), periodically duplicated according to the moiré superlattice positions (see supporting information):

$$U_{\text{lat}}(x, y) = \frac{U_{\text{lat0}}}{2} + \frac{U_{\text{lat0}}}{2} \cos\left(2\pi \frac{\sqrt{x^2 + y^2}}{a_{\text{lat}}}\right), \quad \text{for} \quad x^2 + y^2 \leqslant \frac{a_{\text{lat}}^2}{4} \text{ in a single period} \tag{1}$$

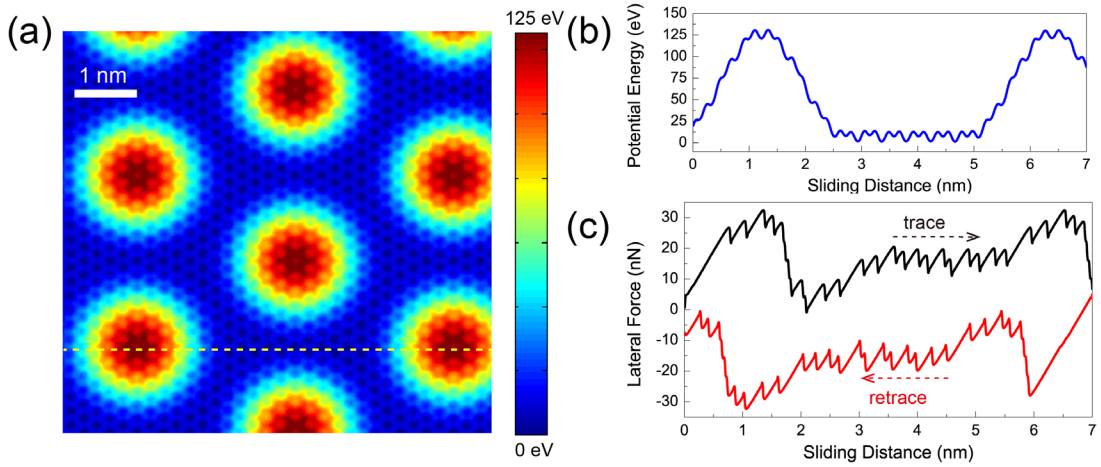


**Figure 2.** (a) Potential energy surface applied in Prandtl–Tomlinson (PT) calculation according to equations (1)–(2), where $U_{lat0} = 16$ eV, $U_{sup0} = 120$ eV, $a_{lat} = 2.5$ Å, $a_{sup} = 30$ Å. (b) and (c) Potential energy variation and the corresponding friction loop on the dashed line in (a).

$$U_{sup}(x,y) = \frac{U_{sup0}}{2} + \frac{U_{sup0}}{2}\cos\left(2\pi\frac{\sqrt{x^2+y^2}}{a_{sup}}\right),$$
$$\text{for} \quad x^2+y^2 \leqslant \frac{a_{sup}^2}{4} \text{ in a single period} \qquad (2)$$

where $U_{lat0}$ and $U_{sup0}$ are the depth of potential $U_{lat}$ and $U_{sup}$, $a_{lat}$ and $a_{sup}$ are the width of $U_{lat}$ and $U_{sup}$, respectively.

By using a method similar to previous studies [34, 45, 47], a friction loop with the same feature of dual-wavelength stick-slip is obtained as shown in figure 2(c), along the dashed scanning line in figure 2(a) with potential energy profile in figure 2(b). Instead of smooth friction modulation, the friction loop clearly exhibited superlattice-level slip instability. For stick-slip to occur at both atomic and superlattice scales, a substantially enhanced energy barrier is required at the superlattice level [48]. In other words, $U_{sup0}/a_{sup}$ should be large enough (comparable to $U_{lat0}/a_{lat}$) to enable the superlattice-level stick-slip. By gradually decreasing the ratio of $U_{sup0}/U_{lat0}$, a transition from long-range stick-slip to smooth long-range modulation was obtained (see Supporting Information). To verify this point, a similar system of graphene epitaxially grown on another transition metal substrate Ir(1 1 1), was tested both experimentally and theoretically (see supporting information). The dual-scale stick-slip friction is not observable on graphene/Ir(1 1 1) substrate, we attributed this absence of superlattice-level slip instability to a much lower potential energy barrier $U_{sup0}$, which is confirmed by the comparison of superlattice-level sliding energy barriers between graphene/Ru(0 0 0 1) and graphene/Ir(1 1 1) systems by DFT calculations in the next section.

Based on the numerical calculation, the long-range energy barrier ($U_{sup0}$) has led to the superlattice-level slip instability on graphene/Ru(0 0 0 1) heterostructure. In order to unravel the physical origins of this superlattice-level potential, DFT calculations were carried out to compute the potential energy surface (PES) experienced by the tip along the sliding path. Figure 3(a) shows the initial configuration of graphene/Ru(0 0 0 1) heterostructure, where four subdivisions can be distinguished according to their different stacking structures. We adopt the definition of the fcc, hcp, atop and bridge regions in which the location of hexagonal holes of the graphene layer are on the fcc hollow, hcp hollow, top and bridge site of the first layer of Ru atoms in the Ru(0 0 0 1) substrate [49]. The morphology of graphene after geometry optimization is shown in figure 3(b). The lattice mismatch and strong interaction between graphene and Ru(0 0 0 1) substrate result in a corrugated structure with 3.0 nm period moiré superlattice and 1.4 Å height humps, which is qualitatively consistent with previous reports [43, 50] and our AFM measurements in Supporting Information. According to figure 3(c), the interfacial charge transfer is facilitated between graphene and Ru by hybridization between C $2p_z$ and Ru $4d_{z^2}$ orbitals at the hcp and fcc regions. Due to this interfacial interaction, the atomic stacking between C and Ru atoms prefers the head-on-head fashion at the flat regions (hcp and fcc) forming a more aligned structure. This forces the atoms to displace towards the center of atop region, and as a consequence the atop region buckles vertically as isolated humps to accommodate the large lattice mismatch between graphene and Ru(0 0 0 1) substrate [51]. It is noted that the C–Ru interaction is relatively weak in the hump region. Subject to the expensive computational cost, a single Ar atom, rather than an actual tip with finite size, was utilized to qualitatively represent the potential energy variation felt by the tip during scanning, which should be physically meaningful as demonstrated in previous studies [52–54]. The sliding path was chosen along the black arrow in figure 3(a) to coincide roughly with the experimental condition as indicated by the blue line in the fast scan direction in figure 1(a). The PES calculation was firstly conducted in a 'constant height mode'

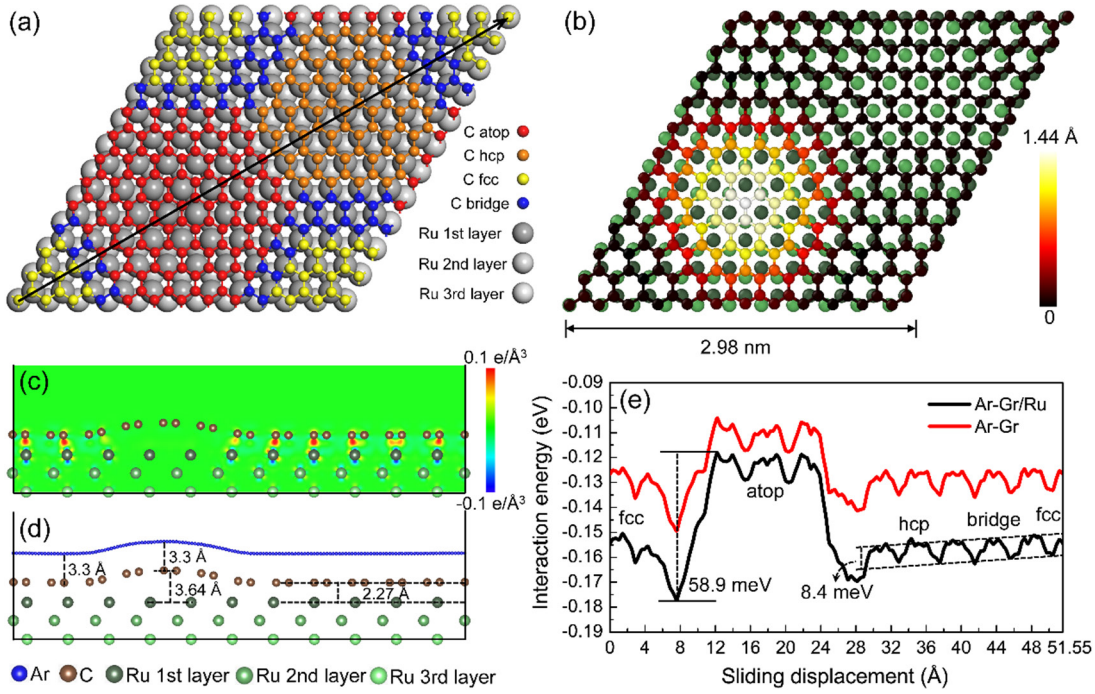


**Figure 3.** (a) A schematic illustration showing different types of carbon atoms with different stacking configurations in one supercell. The black arrow represents the projected scanning path of the Ar atom. (b) Surface morphology after relaxation. The colors on C atoms reflect the topographic corrugation of graphene. (c) Difference charge density, representing charge transfer distributions between graphene and Ru(0 0 0 1) substrate. (d) The trajectory of the Ar atom (blue curve) along the scanning direction (black arrow in (a)) on graphene. (e) The calculated potential energy surface along the scanning direction.

where the distance between the Ar atom and graphene surface was kept constant at 3.3 Å (see the blue trajectory in figure 3(d)) as a first order approximation of the constant-load mode in AFM scanning. During the calculation, no further relaxation is allowed for the structure. Constant-load calculation with relaxed structure is also conducted in the next section to verify the PES estimation here.

Because it is the variation rather than the absolute value of potential energy that matters, the interaction energy surface (IES) is adopted, where the total Ar/substrate energy is subtracted by the self-energies of Ar atom and substrate as described in Supporting Information. The IES along the path, denoted by $U_{\text{hetero}}$, is shown as the black curve in figure 3(e), where two energy corrugation modes can be clearly observed. The weaker energy corrugation with an amplitude of 8.4 meV has a period coinciding with the graphene lattice periodicity along the armchair direction and it is responsible for the atomic-level stick-slip process. Meanwhile a stronger potential energy barrier with an amplitude of 58.9 meV can also be observed in each period of the moiré superlattice structure. The high energy states correspond to the positions when the Ar atom is located above the hump of graphene. The variation of the strong energy barrier occurs around the atop region while the potential remains relatively steady at the fcc, hcp and bridge regions.

To reveal the origin of superlattice-level potential energy corrugation, we further considered the individual contribution of interactions to the total potential energy. As shown by the red curve in figure 3(e), the total energy corrugation is dominated by the interaction energy between the Ar atom and graphene. Therefore, the deformation and curvature of the graphene sheet plays an essential role in forming the high sliding energy barrier. Previous studies indicated that the Schwöbel barrier originating from the asymmetric potential well accompanying the step edge could significantly affect the atomic friction force [52, 53]. Similarly, we found that the superlattice-level potential energy corrugation is largely ascribed to the existence of the corrugated hump structure, which is geometrically very steep acting as an obstacle opposing the tip sliding, rather than the electronic corrugation, i.e. the inhomogeneous distribution of the interfacial charge transfer as indicated in figure 3(c). The formation of this hump structure is a combined effect of both lattice mismatch and covalent interaction through significant charge transfer in the aligned regions (hcp and fcc) between graphene and Ru(0 0 0 1), which should also apply to graphene on other strongly interacting substrates. However, the superlattice-level sliding energy barrier on graphene/Ir(1 1 1) substrate is found to be much smaller by DFT calculations (see supporting information). With weak van der Waals interaction between graphene and Ir(1 1 1) substrate, a very smooth rather than corrugated morphology is favored for graphene/Ir(1 1 1) substrate, which avoids the huge sliding barrier and superlattice-level slip instability.

The simulation results in figure 3(e) present the variation of interaction energy of the rigid structure during

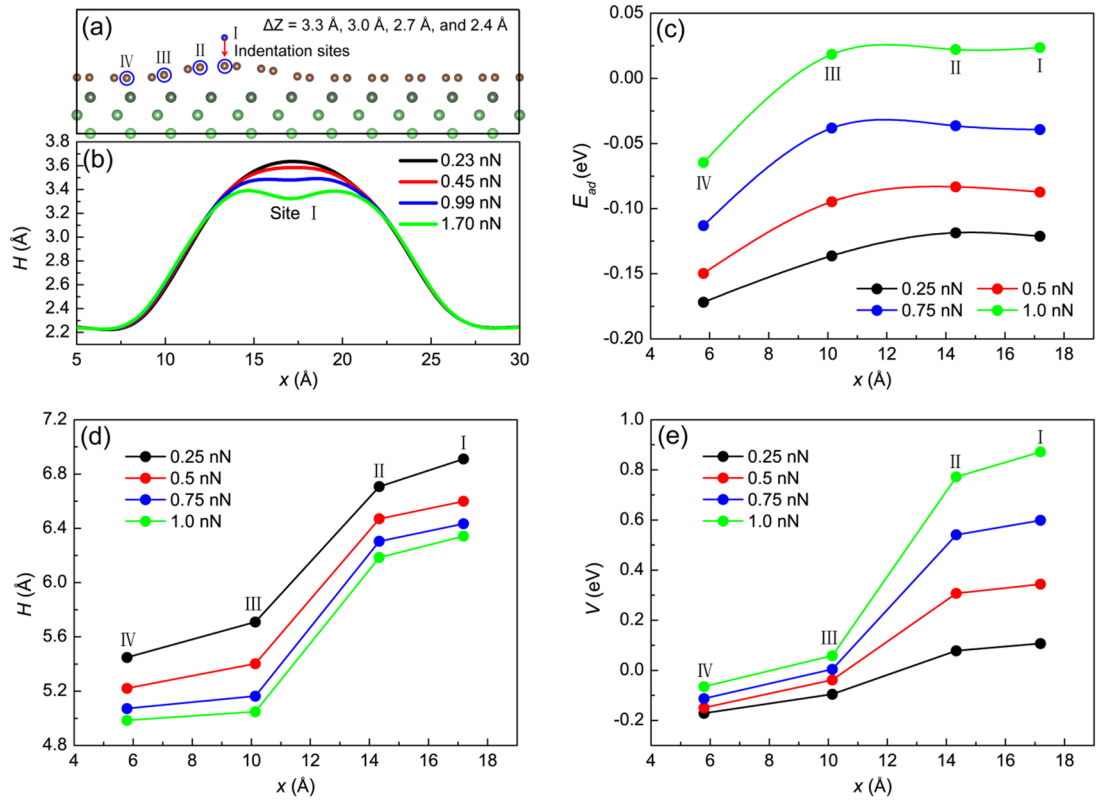


**Figure 4.** Indentation processes of an Ar atom on specific sites of the atop and fcc regions in graphene with a head on head fashion between Ar and C atoms to simulate the climbing process of Ar atom under external force. (a) the schematic of indentation process of the Ar atom on the graphene at the specific sites labelled as I, II, III, and IV; (b) the morphology evolution of graphene during the indentation of Ar atom on the site I of graphene; (c) the adsorption energy at the C atoms labelled as I, II, III, and IV under 0.25 nN, 0.5 nN, 0.75 nN, and 1 nN. (d) the relative height of Ar atom under the load of 0.25 nN, 0.5 nN, 0.75 nN, and 1 nN at specific sites I, II, III, and IV in graphene; the height of top layer of Ru substrate was set to zero as a reference for both (b) and (d); (e) the total potential energy of the system including the configuration energy and the work of external force on Ar atom during the sliding process.

scanning. However, in real experiments, the graphene layer is subjected to normal loads exerted by the AFM tip and thus unavoidable deformation. In a recent study, the humps formed in graphene/Ru(0 0 0 1) heterostructure were found to be deformable under nanoindentation by noncontact AFM [22]. To explore the effect of hump deformation on potential energy corrugation, we kept the graphene and the first Ru (0 0 0 1) layer relaxed and gradually indented the Ar atom towards graphene at various carbon atom sites labelled as I, II, III, and IV (figure 4(a)) respectively. The distances between Ar atom and labelled C atoms, or simply 'Ar heights ($\Delta Z$)' were selected to be 3.3 Å, 3.0 Å, 2.7 Å, and 2.4 Å to simulate the indentation process. The adsorption energy ($E_{ad}$) and external force ($f_{ext}$) of the Ar atom is calculated at each C atom site and Ar height, where the adsorption energy is defined by [54].

$$E_{ad} = E(\text{Ar} - \text{Gr/Ru}) - E(\text{Ar}) - E(\text{Gr/Ru}) \quad (3)$$

where $E$(Ar–Gr/Ru), $E$(Ar) and $E$(Gr/Ru) are relaxed energies of the entire system, the isolated Ar atom and the Gr/Ru(0 0 0 1) substrate, respectively.

The morphologies of graphene when the Ar atom indents at different sites with different indentation depths are shown in figures 4(b) and S11. As shown in figure 4(b), the hump of graphene keeps nearly intact at normal loads less than 0.45 nN, and a dent begins to appear in the hump as the force further increases. However even the normal load reaches up to the value of 1.70 nN (corresponding to a local contact pressure of more than 10 GPa), the hump is still relatively higher than the surrounding regions. It should be mentioned that the value of normal load shown here is exerted on a single Ar atom, which should add up to a much larger load in real experiment, where a large number of atoms are in contact between AFM tip and the sample. This suggests that the locally corrugated configuration can robustly resist the compression by the tip even under high normal loading, which could be attributed to the covalent interaction between graphene and Ru(0 0 0 1) in hcp and fcc regions.

In order to simulate the constant-load mode in real AFM experiments, the adsorption energy and the indentation depth of the Ar atom at a series of normal loads (i.e. 0.25 nN, 0.5 nN, 0.75 nN, and 1 nN) were obtained by interpolation (See Supporting Information and figure S12) with tolerable errors [55]. Both the adsorption energy ($E_{ad}$) and the indentation depth ($H$) are dependent on the normal load ($f_{ext}$) and the indentation sites ($x$), as shown in figures 4(c) and (d), respectively.

According to previous studies [54], the potential energy $V$ (figure 4(e)) of a system under an external normal loading has two main components, i.e.

variations of adsorption energy, and the work against the external force $f_{ext}$ applied to Ar atom due to variations of the indentation depth:

$$V(x, f_{ext}) = E_{ad}(x, H(x, f_{ext})) + f_{ext} \cdot H(x, f_{ext}) \quad (4)$$

By comparison of figures 4(c)–(e), we find that the work done by the external load due to the uphill motion dominates the potential energy barrier during the sliding process, while the adsorption energy differences play only a relatively minor role. Furthermore, the potential energy barrier associated with the hump is enhanced when the normal load increases from 0.25 nN to 1 nN. This again verifies the importance of the corrugated morphology of graphene in determining the moiré superlattice-level stick-slip frictional behavior.

With this, we could try to answer the questions raised in the Introduction section. Firstly, the moiré superstructure could indeed invoke the long-range stick-slip instabilities on 2D materials, given that 'super-potential' corrugation is large enough to meet the instability criterion [48]. As the moiré period is generally more than 10 times the lattice period, the 'super-potential' should be much larger than the atomic potential in order for the dual-scale stick-slip behaviors to occur simultaneously. Secondly, the physical origin of the 'super-potential' has been elucidated by DFT calculations. According to the above analyses, the essential role of morphological corrugation (figures 3(e) and S10), as well as the dominant role of uphill work done by external load (figures 4(c) and (e)), suggests that the moiré 'super-potential' corrugation experienced by the scanning atom mainly originates from geometric corrugation, rather than the electronic corrugation of 2D heterostructures, even when the interfacial charge transfer is strongly inhomogeneous over the scanning area. This also predicts the transition from significant superlattice-level stick-slip instability to continuous friction modulation by reducing the geometrical corrugation of graphene, which has been verified in the present study by comparing the strongly corrugated graphene/Ru(0 0 0 1) with ultrasmooth graphene/Ir(1 1 1) systems. Thirdly, the morphological corrugation depends on both factors of the interfacial interaction and lattice mismatch between 2D materials and their underlying substrate. Strong interfacial interaction is a prerequisite to combat the elastic energy of 2D materials and enable significant in-plane and out-of-plane deformation, while sufficient lattice mismatch is required to form moiré superstructure. If the lattice mismatch is negligibly small, the moiré pattern will not be observable by compulsory strain (e.g. graphene/Ni(1 1 1)) when the 2D materials are covalently bound to the substrate; or a very large-period moiré pattern will emerge with gentle morphological corrugation (e.g. graphene/h-BN) when the interfacial interaction is primarily weak van der Waals interactions.

## 4. Conclusions

In summary, an unusual moiré superlattice-level stick-slip was observed on graphene/Ru(0 0 0 1) heterostructure, in addition to the regular atomic-scale stick-slip friction. The emergence of the superlattice-level slip instability could cause hysteresis in friction loop and hence an additional energy dissipation mode. According to the classic PT model, this superlattice-level slip instability must be associated with a huge sliding energy barrier. The superlattice-level potential energy corrugation is found to arise from the corrugated morphology of graphene, which originates from the strong interfacial electronic interaction between graphene and Ru(0 0 0 1) substrate. The hump of graphene has been verified to be robust even under sliding contact with high normal pressure. Thanks to the strong interfacial adhesion, the regular corrugated morphology, and the consistent lattice alignment over a large area, graphene/Ru(0 0 0 1) heterostructure could be used potentially as a template for both fundamental researches and technological applications, i.e. to reveal the mechanism of frictional energy dissipation, and to obtain sub-nanometer positioning and alignment accuracy. We could also predict that 2D materials on other strongly interacting substrates with suitable lattice mismatch, like graphene/Re(0 0 0 1) could also possess the dual-scale stick-slip friction behavior [56, 57]. This work proposes a potential strategy by tuning the interfacial interaction between graphene and underlying substrate to control frictional and mechanical properties of these 2D materials.

## Acknowledgments

The authors would like to acknowledge the helpful discussions with Zijian Wang, and support of the National Natural Science Foundation of China (Grant Nos. 51422504, 11422218, 51325204, 61504149, 11272177, 51527901, 51375010, 11432008), the National Key Basic Research Program of China (2013CB934200, 2013CB933003, 2015CB351903), the Tsinghua University Initiative Scientific Research Program (2014Z01007), the President Funds of University of Chinese Academy of Sciences. Simulations were carried out on the 'Explorer 100' cluster system of Tsinghua National Laboratory for Information Science and Technology.

## References

[1] Park J Y and Salmeron M 2013 *Chem. Rev.* **114** 677–711
[2] Carpick R W 2006 *Science* **313** 184–5
[3] Lee C, Li Q, Kalb W, Liu X Z, Berger H, Carpick R W and Hone J 2010 *Science* **328** 76–80
[4] Novoselov K S, Geim A K, Morozov S V, Jiang D, Zhang Y, Dubonos S V, Grigorieva I V and Firsov A A 2004 *Science* **306** 666–9
[5] Ponomarenko L A *et al* 2013 *Nature* **497** 594–7
[6] Zhang Y, Tan Y, Stormer H L and Kim P 2005 *Nature* **438** 201–4
[7] Zhu M *et al* 2016 *2D Mater.* **4** 011013

[8] Kim K S, Lee H J, Lee C, Lee S K, Jang H, Ahn J H, Kim J H and Lee H J 2011 *ACS Nano* **5** 5107–14
[9] Spear J, Custer J and Batteas J 2015 *Nanoscale* **7** 10021–9
[10] Sen H S, Sahin H, Peeters F M and Durgun E 2014 *J. Appl. Phys.* **116** 083508
[11] Deng Z, Smolyanitsky A, Li Q, Feng X-Q and Cannara R J 2012 *Nat. Mater.* **11** 1032–7
[12] Li S, Li Q, Carpick R W, Gumbsch P, Liu X Z, Ding X, Sun J and Li J 2016 *Nature* **539** 541–5
[13] Koren E, Leven I, Lörtscher E, Knoll A, Hod O and Duerig U 2016 *Nat. Nanotechnol.* **11** 752–7
[14] Filleter T, McChesney J L, Bostwick A, Rotenberg E, Emtsev K, Seyller T, Horn K and Bennewitz R 2009 *Phys. Rev. Lett.* **102** 086102
[15] Li Q, Liu X Z, Kim S P, Shenoy V B, Sheehan P E, Robinson J T and Carpick R W 2014 *Nano Lett.* **14** 5212–7
[16] Koren E, Lörtscher E, Rawlings C, Knoll A W and Duerig U 2015 *Science* **348** 679–83
[17] Geim A K and Grigorieva I V 2013 *Nature* **499** 419–25
[18] Van Wijk M M, Schuring A, Katsnelson M I and Fasolino A 2015 *2D Mater.* **2** 034010
[19] Guo W, Yin J, Qiu H, Guo Y, Wu H and Xue M 2014 *Friction* **2** 209–25
[20] Kawai S *et al* 2016 *Science* **351** 957–61
[21] Zhang K *et al* 2015 *Nano Lett.* **15** 6586–91
[22] Koch S *et al* 2013 *ACS Nano* **7** 2927–34
[23] Decker R, Wang Y, Brar V W, Regan W, Tsai H Z, Wu Q, Gannett W, Zettl A and Crommie M F 2011 *Nano Lett.* **11** 2291–5
[24] Hong X, Kim J, Shi S F, Zhang Y, Jin C, Sun Y, Tongay S, Wu J, Zhang Y and Wang F 2014 *Nat. Nanotechnol.* **9** 682–6
[25] Woods C R *et al* 2014 *Nat. Phys.* **10** 451–6
[26] Ouyang W, Ma M, Zheng Q and Urbakh M 2016 *Nano Lett.* **16** 1878–83
[27] Tang S *et al* 2015 *Nat. Commun.* **6** 6499
[28] Wang L, Ma T, Hu Y, Zheng Q, Wang H and Luo J 2014 *Nanotechnology* **25** 385701
[29] Yang W *et al* 2013 *Nat. Mater.* **12** 792–7
[30] Zheng X *et al* 2016 *Nat. Commun.* **7** 13204
[31] Chan N, Balakrishna S G, Klemenz A, Moseler M, Egberts P and Bennewitz R 2017 *Carbon* **113** 132–8
[32] Filleter T and Bennewitz R 2010 *Phys. Rev.* B **81** 155412
[33] Maier S, Gnecco E, Baratoff A, Bennewitz R and Meyer E 2008 *Phys. Rev.* B **78** 045432
[34] Steiner P, Gnecco E, Filleter T, Meyer E, Bennewitz R and Afm S Á 2010 *Tribol. Lett.* **39** 321–7
[35] Butt H J and Jaschke M 1995 *Nanotechnology* **6** 1
[36] Li Q, Kim K S and Rydberg A 2006 *Rev. Sci. Instrum.* **77** 065105
[37] Carpick R W, Ogletree D F and Salmeron M 1997 *Appl. Phys. Lett.* **70** 1548
[38] Kresse G and Furthmüller J 1996 *Phys. Rev.* B **54** 11169–86
[39] Blöchl P E 1994 *Phys. Rev.* B **50** 17953–79
[40] Klimes J, Bowler D R and Michelides A 2011 *Phys. Rev.* B **83** 195131
[41] Klimes J, Bowler D R and Michelides A 2010 *J. Phys.: Condens. Matter* **22** 022201
[42] Björkman T 2014 *J. Chem. Phys.* **141** 074708
[43] Jiang D E, Du M H and Dai S 2009 *J. Chem. Phys.* **130** 074705
[44] Pan Y, Zhang H, Shi D, Sun J, Du S, Liu F and Gao H J 2009 *Adv. Mater.* **21** 2777–80
[45] Dong Y, Vadakkepatt A and Martini A 2011 *Tribol. Lett.* **44** 367–86
[46] Tomlinson G A 1929 *Phil. Mag.* **7** 905
[47] Wang Z, Ma T, Hu Y, Xu L and Wang H 2015 *Friction* **3** 170–82
[48] Socoliuc A, Bennewitz R, Gnecco E and Meyer E 2004 *Phys. Rev. Lett.* **92** 134301
[49] Zhang L Z *et al* 2014 *Adv. Mater. Interfaces* **1** 1300104
[50] Wang B, Bocquet M L, Marchini S, Günther S and Wintterlin J 2008 *Phys. Chem. Chem. Phys.* **10** 3530
[51] Gao L, Liu Y, Ma T, Shi R, Hu Y and Luo J 2016 *Appl. Phys. Lett.* **108** 261601
[52] Steiner P, Gnecco E, Krok F, Budzioch J, Walczak L, Konior J, Szymonski M and Meyer E 2011 *Phys. Rev. Lett.* **106** 186104
[53] Hölscher H, Ebeling D and Schwarz U D 2008 *Phys. Rev. Lett.* **101** 246105
[54] Zhong W and Tomanek D 1990 *Phys. Rev. Lett.* **64** 3054
[55] Cahangirov S, Ataca C, Topsakal M, Sahin H and Ciraci S 2012 *Phys. Rev. Lett.* **108** 126103
[56] Miniussi E, Pozzo M, Baraldi A, Vesselli E, Zhan R, Comelli G, Menteş T O, Niño M A, Locatelli A and Lizzit S 2011 *Phys. Rev. Lett.* **106** 216101
[57] Gao L, Liu Y, Shi R, Ma T, Hu Y and Luo J 2017 *RSC Adv.* **7** 12179–84